ISSN 1063-780X, Plasma Physics Reports, 2013, Vol. 39, No. 2, pp. 167–182. © Pleiades Publishing, Ltd., 2013.
Original Russian Text © A.N. Trushkin, M.E. Grushin, I.V. Kochetov, N.I. Trushkin, Yu.S. Akishev, 2013, published in Fizika Plazmy, 2013, Vol. 39, No. 2, pp. 193–209.

LOW-TEMPERATURE PLASMA

Decomposition of Toluene in a Steady-State Atmospheric-Pressure Glow Discharge

A. N. Trushkin, M. E. Grushin, I. V. Kochetov, N. I. Trushkin, and Yu. S. Akishev

Troitsk Institute for Innovation and Fusion Research, Troitsk, Moscow, 142092 Russia

Received April 22, 2012; in final form, July 19, 2012

Abstract—Results are presented from experimental studies of decomposition of toluene ($C_6H_5CH_3$) in a polluted air flow by means of a steady-state atmospheric pressure glow discharge at different water vapor contents in the working gas. The experimental results on the degree of $C_6H_5CH_3$ removal are compared with the results of computer simulations conducted in the framework of the developed kinetic model of plasma chemical decomposition of toluene in the $N_2 : O_2 : H_2O$ gas mixture. A substantial influence of the gas flow humidity on toluene decomposition in the atmospheric pressure glow discharge is demonstrated. The main mechanisms of the influence of humidity on $C_6H_5CH_3$ decomposition are determined. The existence of two stages in the process of toluene removal, which differ in their duration and the intensity of plasma chemical decomposition of $C_6H_5CH_3$ is established. Based on the results of computer simulations, the composition of the products of plasma chemical reactions at the output of the reactor is analyzed as a function of the specific energy deposition and gas flow humidity. The existence of a catalytic cycle in which hydroxyl radical OH acts a catalyst and which substantially accelerates the recombination of oxygen atoms and suppression of ozone generation when the plasma-forming gas contains water vapor is established.

DOI: 10.1134/S1063780X13020025

1. INTRODUCTION

Volatile organic compounds (VOC) including toluene ($C_6H_5CH_3$) form a large group of ecologically dangerous components contained in the exhaust gas flows of various processes in chemical, textile, food, lumber, electro-technical, and other industries. The specificity and complexity of purification of the exhaust gas from VOC vapors consists in the fact that the purification efficiency depends substantially on the chemical nature of each particular organic compound. The acute problem is further complicated by the necessity of processing large-volume flows of polluted gas containing low concentration of hazardous compounds. One of the prospective methods of solving these problems consists in processing polluted gas flows by means of nonequilibrium low-temperature atmospheric-pressure plasma. However, successful introduction of new plasma technologies of gas purification into practice requires solving two important problems: lowering energy consumption and achieving possibly complete oxidation of complex carbohydrates down to carbon dioxide and water. Obviously, in order to solve both problems, a better understanding of all stages of plasma chemical decomposition of complex carbohydrates is needed, as well as determination of parameters and stages of the process, which are essential for its efficiency. Experimental studies of detailed kinetics of plasma chemical removal of complex carbohydrates at atmospheric pressure are hindered by the abundance of intermediate products, many of which exhibit high chemical activity and, correspondingly, a short lifetime. Under such circumstances, detailed numerical modeling of the plasma chemical processes is of crucial importance for establishing the kinetic patterns.

A detailed kinetic model of plasma chemical decomposition of toluene in a gas mixture of nitrogen and oxygen ($N_2 : O_2$) was developed in [1]. Numerical simulations based on this model showed that the hydroxyl radical OH that is produced in the gas medium due to plasma chemical reactions between the products of $C_6H_5CH_3$ decomposition and atoms and molecules of oxygen substantially contributes to decomposition of $C_6H_5CH_3$ in the presence of oxygen in the plasma-forming gas. Since in reality exhaust gas flows frequently contain water vapor, it is natural to assume that the presence of moisture in polluted gas will have a noticeable influence both on the efficiency of toluene removal and composition of final products of its destruction. It should be noted that researchers working on the development of plasma chemical methods of gas purification do not currently have a common opinion on the character and degree of the influence of water vapor on the process of toluene removal. A large number of experimental investigations on the influence of humidity on the efficiency of plasma chemical removal of $C_6H_5CH_3$ are described in the literature. However, the results are frequently inconsistent. There are three points of view regarding the problem under consideration [2]: (i) the presence of water vapor in the plasma-forming gas increases the

efficiency of $C_6H_5CH_3$ decomposition [3–10], (ii) humidity has no influence on the process of gas purification from toluene [11], and (iii) H_2O vapor negatively influences the efficiency of $C_6H_5CH_3$ decomposition [12, 13]. The existence of the optimal concentration of water vapor for which removal of toluene reaches its maximum was reported in [6, 7, 10]. The value of this concentration $[H_2O]_{opt}$ varies between 0.2 and 5% (vol.).

The experiment shows that H_2O vapor can influence the efficiency of toluene removal through several channels. The presence of water vapor in the plasma-forming gas opens direct mechanisms of hydroxyl radical production via electron-impact dissociation of H_2O molecules (in the active discharge stage) or collisions of H_2O molecules with electronically excited atoms and molecules (in the active and afterglow stages).

It can be expected that, for fixed parameters of the discharge, the number of produced OH radicals will increase with increasing vapor concentration $[H_2O]$, which should increase the efficiency of $C_6H_5CH_3$ decomposition. This assumption is partially confirmed by the experimental results of [14], where it was shown that the concentration of the hydroxyl radical [OH] in a pulsed streamer corona increases linearly as the $[H_2O]$ content increases to $[H_2O] \approx 1\%$. However, at $[H_2O] > 1\%$, the rate of increase in the OH concentration in the discharge substantially slows down.

The other channel through which water vapor can affect the process of removal of $C_6H_5CH_3$ is related to the influence of molecules of H_2O on the value of the reduced electric field E/N (where E is the electric field strength and N is the number density of neutral particles) [4], electron density, ion current, and spatiotemporal characteristics of the discharge itself. It was shown in [15] that the presence of water vapor in the gas mixture leads to a noticeable decrease in the number of microdischarges in the dielectric barrier discharge, and, correspondingly, to a decrease in the volume of the working gas. Since water vapor is an electronegative admixture, activation of an additional channel for consumption of electrons via their dissociative attachment to the H_2O molecule leads to a reduction in the electron density (i.e., to a reduction in the total discharge current for a given electric field strength in the discharge, or to an increase in the electric field strength for a fixed current value), and, correspondingly, to a decrease in the quantity of the produced chemically active particles. In a real experiment, both of the above mentioned channels act simultaneously. In this case, the end result of the influence of water vapor is not obvious a priori and depends on the composition of the working gas and the type of the used generator of nonequilibrium low-temperature plasma.

In this work, we present the results of experimental studies on removal of toluene from a polluted air flow by means of a steady-state atmospheric pressure glow discharge at different water vapor contents in the working gas. We compare experimental data on the degree of $C_6H_5CH_3$ removal with the results of computer simulation performed within the framework of the developed kinetic model of plasma chemical decomposition of toluene in the $N_2 : O_2 : H_2O$ gas mixture. Based on the results of the computer simulation, we analyze the composition of products of the plasma chemical reactions at the output of the reactor as a function of specific energy deposition and humidity of the gas flow.

Plasma purification of polluted gas flows that contain oxygen-containing components (O_2, H_2O, CO_2, etc.) from volatile organic compounds is realized by consecutive oxidation of initial toxic compounds, which results in stable final products, such as carbon dioxide CO_2 and water H_2O. The first step in such decomposition of VOC vapors via oxidation consists in interaction of an organic molecule of the toxic substance with active particles produced in plasma (atomic oxygen O, hydroxyl radical OH, etc.). As a result of this interaction, a molecule of a passive organic VOC gets transformed into an active radical of a carbohydrate, which enters a chain of successive plasma chemical reactions. To denote this process, we will use three equal terms: "decomposition," "destruction," and "removal." The first two terms will be used mainly when describing the kinetics of plasma chemical transformations of toluene, whereas the third term ("removal") will be used when describing the final, integral results of gas purification, such as energy efficiency of the process, the degree of purification, etc.

2. EXPERIMENTAL

Experimental studies of the toluene removal were conducted in the gas-discharge chamber (GDC). Its construction was described in detail in [16]. The general layout of the experiment is illustrated in Fig. 1.

Nonequilibrium low-temperature plasma was created in the air flow by means of the self-sustained atmospheric-pressure glow discharge in the GDC with a cross section of 20 cm^2 and length along the flow of 30 cm. The gas was blown perpendicular to the direction of electric current. The electrode system of the GDC consisted of a cathode block in the form of a stack protruding into the gas flow rods and a continuous anode plate with spherical wells. The axial line of each cathode rod was aligned with the corresponding well of the anode plate. Each cathode rod had several emitting sections and was connected to the voltage source through an individual ballast resistor. In the presented experiments, the maximum number of the used electrode pairs (a cathode rod and an anode well)

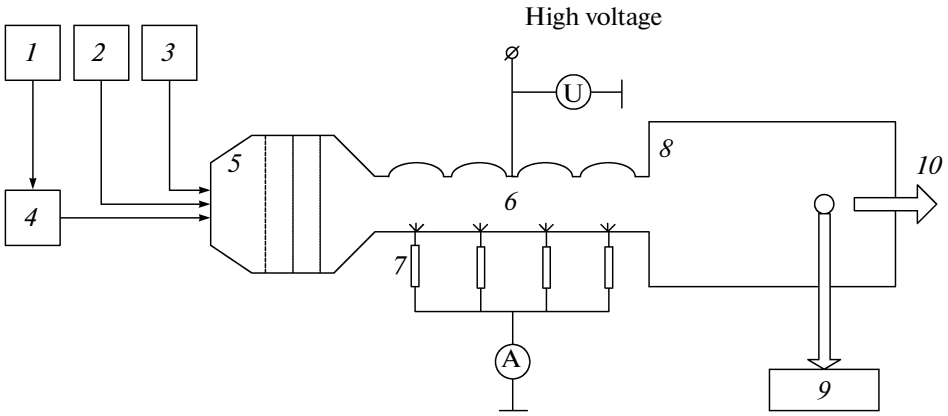

Fig. 1. Experimental arrangement: (*1*) air inlet, (*2*) steam generator, (*3*) barbotage column for generation of toluene vapor, (*4*) air heater, (*5*) mixing chamber, (*6*) gas-discharge chamber, (*7*) ballast resistors, (*8*) plasma chemical reactor, (*9*) chromatograph, and (*10*) air pumping system.

was 28 and the distance between the emitting cathode section and the surface of the anode well was 1.35 cm.

This system of electrodes allowed obtaining the gas discharge in different regimes: at low currents, the discharge at each rod existed in the form of a negative corona (this form of the discharge was not used for toluene removal), while at higher currents, the corona evolved into a uniform glow discharge. It should be noted that, at moderate velocity of the flow $V = 15$–20 m/s, the average (divided by the anode area) current density in the glow discharge did not exceed $j = 1$ mA/cm^2, which was limited by the transition of the glow discharge into a spark discharge. At high flow velocity $V = 100$ m/s, it was possible to increase the current density in the glow discharge to $j > 10$ mA/cm^2 [17].

The volume content of water vapor ε in the air flow varied from 1.2 to 18%. Experiments were conducted at two initial concentrations of toluene: 15 and 125 ppm. In the experiments with a moisture content of 1.2 and 10%, the specific energy deposition was varied by changing the length of the discharge along the flow. The length of the discharge was varied by changing the number of cathode elements connected to the voltage source at a constant value of current flowing through each cathode element. In this case, the time of gas exposure to the discharge varied from 3 to 18 ms. The chosen means of varying the specific energy deposition allowed conducting investigation of toluene decomposition at a fixed value of the electric field strength in the discharge. At high ($\varepsilon = 18\%$) water vapor content, the specific energy deposition was varied by changing the discharge current while keeping the number of the cathode elements fixed.

The experimental setup (Fig. 1) also included a fan, a steam generator, a gas heater, and a barbotage column, which were used to achieve the required gas flow parameters, such as the velocity and temperature of the gas mixture and the contents of toluene and water vapor. The air heater, steam generator, mixing chamber, and all gas delivery lines were made of stainless steel and were heated by individual heaters for preventing possible condensation of water and toluene on the walls. The gas-discharge chamber was electrically powered by a dc voltage whose amplitude U was varied between 0 and 30 kV.

After the GDC, the plasma-activated gas flow entered the chemical reactor, where chemical processes of toluene decomposition initiated by the discharge plasma continued. The chemical reactor represented a 1-m-long channel with a rectangular cross section of 25 × 25 cm. The gas flow velocity in the reactor dropped to $V \sim 0.5$ m/s, resulting in a gas passage time through the reactor of about 2 s. Diagnostics of the gas composition was accomplished by means of a gas chromatograph (model 1300) equipped with a flame-ionization detector. We used extension columns from stainless steel with a diameter of 5 mm, length of 5 m, and different sorbents: Porapak Q, Porapak R, molecular sieve, etc. Measurements were conducted both in the regime with constant temperature (80–160°C), and in the regime with a programmed temperature with a different increase rate. The ultimate detectable toluene vapor concentration was about 0.5 ppm.

3. DESCRIPTION OF THE MODEL

In this work, we developed the kinetic model describing decomposition of toluene in a steady-state uniform glow discharge in a flow of humid air at atmospheric pressure. The kinetic equations for charged particles and molecules of the gas mixture being analyzed, both in the ground state and vibrationally and electronically excited states, along with those for secondary products, were solved simultaneously with solution of the Boltzmann equation for the electronic energy distribution function (EEDF) in the two-term

Table 1. Elementary processes with participation of charged particles, complementing the model [1]

No.	Process	Rate constant, cm^3/s, cm^6/s	Source
1	$H_2O + e \longrightarrow H_2O(010) + e$	BE	[21]
2	$H_2O + e \longrightarrow H_2O(100 + 001) + e$	BE	[21]
3	$H_2O + e \longrightarrow H + OH + e$	BE	[21]
4	$H_2O + e \longrightarrow H^- + OH$	BE	[21]
5	$H_2O + e \longrightarrow H_2 + O^-$	BE	[21]
6	$H_2O + O_2 + e \longrightarrow H_2O + O_2^-$	1.0×10^{-30}	[18]
7	$H_2O + e \longrightarrow H_2O^+ + e + e$	BE	[21]
8	$H_3O^+ + O_2^- \longrightarrow H_2O + O_2 + H$	2.0×10^{-6}	[18]
9	$OH^- + H_3O^+ \longrightarrow H_2O + H_2O$	2.0×10^{-6}	[18]
10	$O^- + H_3O^+ \longrightarrow H_2O + OH$	2.0×10^{-6}	[18]
11	$O_3^- + O_3H_2^+ \longrightarrow O_2 + H_2O + O_3$	1.5×10^{-6}	[18]
12	$O_4^+ + H_2O \longrightarrow O_3H_2^+ + O_2$	1.5×10^{-9}	[18]
13	$O_3^- + H_3O^+ \longrightarrow O_2 + H_2O + OH$	1.9×10^{-6}	[18]
14	$H^- + H_3O^+ \longrightarrow H_2O + H_2$	1.0×10^{-6}	[18]
15	$NO_2^- + H_3O^+ \longrightarrow H_2O + H + NO_2$	1.0×10^{-6}	[18]
16	$O_3H_2^+ + H_2O \longrightarrow H_3O^+ + OH + O_2$	3.0×10^{-10}	[18]
17	$H^- + H_2O \longrightarrow OH^- + H_2$	3.8×10^{-9}	[18]
18	$H_2O^+ + O_2 \longrightarrow O_2^+ + H_2O$	4.3×10^{-10}	[22]
19	$H_2O^+ + H_2O \longrightarrow H_3O^+ + OH$	1.7×10^{-9}	[18]
20	$H^- + N_2O \longrightarrow OH^- + N_2$	1.1×10^{-9}	[18]
21	$H^- + NO_2 \longrightarrow NO_2^- + H$	2.9×10^{-9}	[18]
22	$H_2O^+ + C_6H_5CH_3 \longrightarrow C_6H_5CH_3H^+ + OH$	2.2×10^{-9}	[23]
23	$H_3O^+ + C_6H_5CH_3 \longrightarrow C_6H_5CH_3H^+ + H_2O$	2.2×10^{-9}	[23]
24	$OH^- + O \longrightarrow HO_2 + e$	2.0×10^{-10}	[18]
25	$OH^- + H \longrightarrow H_2O + e$	1.0×10^{-9}	[18]
26	$OH^- + N \longrightarrow HNO + e$	1.0×10^{-11}	[18]
27	$H^- + O_2 \longrightarrow HO_2 + e$	1.5×10^{-9}	[18]
28	$H^- + NO \longrightarrow HNO + e$	4.6×10^{-10}	[18]
29	$OH^- + NO \longrightarrow HNO_2 + e$	1.0×10^{-9}	[18]

Note: BE stands for the rate constants determined by solving the Boltzmann equation governing the electron energy distribution function. Cross sections for electron scattering from H_2O molecule for processes (1)–(5) and (7) are taken from [21]. The rate constants of processes are given in units of cm^3/s and cm^6/s for two- and three-particle processes, respectively.

approximation. Our analysis was based on plasma chemical reactions used in the model of $C_6H_5CH_3$ conversion in dry $N_2 : O_2$ gas mixtures [1], and the model of atmospheric pressure glow discharge in humid air [18]. When describing the excitation kinetic of electronic states of nitrogen, we introduced three electronic levels [1]. The first level corresponds to the lower metastable $N_2(A^3\Sigma_u^+)$ level, the second one corresponds to the sum of metastable level $N_2(a'^1\Sigma_u^-)$ and levels $N_2(a^1\Pi_g)$ and $N_2(w^1\Delta_u)$, and the third effective level $N_2(E_{sum})$ corresponds to the sum of other electronic levels ($N_2(B^3\Pi_g)$, $N_2(C^3\Pi_u)$). Note that a number of processes involving molecules and atoms H_2O, OH, HO_2, H_2O_2, and H were already included in the model [1]. The main processes involving the above listed particles are presented in Tables 1 and 2. Excited molecules $N_2(B^3\Pi_g)$ are the major contributing factor to the $N_2(E_{sum})$ state. The rate of quenching of this state by a water molecule was measured in [19], but the channels causing this quenching were not determined.

Table 2. Elementary processes between neutral particles with participation of molecules of water and its derivatives included in model [1]

No.	Process	A	n	E_a	Source
1	$N_2(A^3\Sigma_u^+) + H_2O \longrightarrow OH + N_2 + H$	5.0×10^{-14}	0	0	[18]
2	$N_2(a'^1\Sigma_u^-) + H_2O \longrightarrow OH + N_2 + H$	2.0×10^{-10}	0	0	estimate
3	$N_2(E_{sum}) + H_2O \longrightarrow OH + N_2 + H$	2.0×10^{-10}	0	0	estimate
4	$O(^1D) + H_2O \longrightarrow O + H_2O$	1.2×10^{-11}	0	0	[18]
5	$O(^1D) + H_2O \longrightarrow OH + OH$	2.2×10^{-10}	0	0	[18]
6	$O(^1D) + H_2O_2 \longrightarrow HO_2 + OH$	5.3×10^{-10}	0	0	[22]
7	$O + H_2O_2 \longrightarrow OH + HO_2$	1.7×10^{-15}	0	0	[22]
8	$O + NO_2 \longrightarrow NO + O_2$	5.1×10^{-12}	0	−0.40137	[22]
9	$O + H_2O \longrightarrow OH + OH$	1.1×10^{-10}	0	75.7	[22]
10	$O + OH \longrightarrow H + O_2$	2.3×10^{-11}	0	−0.9	[18]
11	$O + HO_2 \longrightarrow OH + O_2$	2.9×10^{-11}	0	−1.7	[18]
12	$O + NO_3 \longrightarrow NO_2 + O_2$	1.0×10^{-11}	0	0	[22]
13	$OH + C_6H_5CH_3 + N_2 \longrightarrow C_6H_5OHCH_3 + N_2$	1.5×10^{-31}	0	−1.5	[24]
14	$OH + C_6H_5CH_3 \longrightarrow H_2O + C_6H_5CH_2$	2.6×10^{-12}	1.0	3.65	[24]
15	$OH + H_2O_2 \longrightarrow HO_2 + H_2O$	1.7×10^{-12}	0	0	[22]
16	$OH + NO_3 \longrightarrow HO_2 + NO_2$	2.6×10^{-11}	0	0	[22]
17	$OH + O_3 \longrightarrow HO_2 + O_2$	1.7×10^{-12}	0	7.82	[22]
18	$OH + CH_3 \longrightarrow H_2O + CH_2$	1.2×10^{-10}	0	11.64	[22]
19	$OH + HCO \longrightarrow CO + H_2O$	5.0×10^{-11}	0	0	[22]
20	$OH + CH_3 + N_2 \longrightarrow CH_3OH + N_2$	4.4×10^{-30}	−0.09	0.2	[24]
21	$OH + CH_4 \longrightarrow H_2O + CH_3$	6.18×10^{-13}	2.0	10.64	[22]
22	$OH + HCN \longrightarrow H_2O + CN$	1.2×10^{-13}	0	3.3	[24]
23	$OH + CH_2O \longrightarrow H_2O + HCO$	5.79×10^{-13}	2.98	−14.55	[22]
24	$OH + CH_2O \longrightarrow H + HCOOH$	2.0×10^{-13}	0	0	[22]
25	$OH + CH_3O \longrightarrow H_2O + CH_2O$	3.0×10^{-11}	0	0	[22]
26	$OH + HCOOH \longrightarrow H_2O + CO_2 + H$	4.5×10^{-13}	0	0	[22]
27	$OH + CH_3COCHO \longrightarrow H_2O + CH_3COCO$	1.5×10^{-11}	0	0	[22]
28	$OH + C_6H_5CHO \longrightarrow C_6H_5CO + H_2O$	1.3×10^{-11}	0	0	[22]
29	$OH + NO_2 + N_2 \longrightarrow HNO_3 + N_2$	2.6×10^{-30}	−2.9	0	[22]
30	$OH + NO_2 + O_2 \longrightarrow HNO_3 + O_2$	1.8×10^{-30}	−2.9	0	[18]
31	$OH + NO_2 \longrightarrow NO + HO_2$	2.3×10^{-11}	0	27.94	[22]
32	$OH + N \longrightarrow NO + H$	4.8×10^{-11}	0	0	[18]
33	$OH + NO + N_2 \longrightarrow HNO_2 + N_2$	6.6×10^{-31}	−2.4	0	[18]
34	$OH + OH \longrightarrow O + H_2O$	1.0×10^{-11}	0	−4.57	[18]
35	$OH + OH + N_2 \longrightarrow H_2O_2 + N_2$	6.9×10^{-31}	0	0	[22]
36	$OH + HNO_2 \longrightarrow H_2O + NO_2$	1.8×10^{-11}	0	−3.2	[18]
37	$OH + N_2O \longrightarrow HNO + NO$	3.8×10^{-17}	0	0	[18]
38	$OH + HNO \longrightarrow NO + H_2O$	7.1×10^{-11}	0	0	[18]
39	$OH + H_2 \longrightarrow H_2O + H$	7.7×10^{-12}	0	8.3	[18]
40	$OH + HNO_3 \longrightarrow NO_3 + H_2O$	1.5×10^{-14}	0	−5.9	[18]
41	$OH + C_2H_2O_2 \longrightarrow HCOOH + HCO$	7.0×10^{-12}	0	0	[25]
42	$OH + H + N_2 \longrightarrow H_2O + N_2$	4.3×10^{-31}	0	0	[18]
43	$OH + C_6H_5 \longrightarrow C_6H_5O + H$	8.3×10^{-11}	0	0	[26]
44	$OH + C_6H_6 \longrightarrow C_6H_5 + H_2O$	2.78×10^{-14}	4.1	−1.26	[22]

Table 2. (Contd.)

No.	Process	A	n	E_a	Source
45	$OH + C_2H_2O_2 \longrightarrow H_2O + HCOCO$	1.1×10^{-11}	0	0	[22]
46	$OH + C_4H_4O_2 \longrightarrow$ products	4.5×10^{-11}	0	0	[22]
47	$OH + C_5H_6O_2 \longrightarrow$ products	5.6×10^{-11}	0	0	[22]
48	$OH + CH_3CO \longrightarrow C_2H_2O + H_2O$	2.0×10^{-11}	0	0	[22]
49	$OH + C_2H_2 \longrightarrow H_2 + HCCO$	1.91×10^{-13}	0	0	[22]
50	$OH + C_6H_5OH \longrightarrow C_6H_5O + H_2O$	4.35×10^{-13}	2.0	−5.49	[22]
51	$OH + C_2H_2O \longrightarrow CO + CH_3O$	1.0×10^{-11}	0	0	[22]
52	$OH + C_4H_3 \longrightarrow C_4H_2 + H_2O$	5.0×10^{-11}	0	0	[26]
53	$OH + C_2H_2 \longrightarrow C_2H_2O + H$	1.0×10^{-13}	0	0	[22]
54	$OH + C_4H_2 \longrightarrow HCO + C_3H_2$	5.0×10^{-12}	0	0	[27]
55	$OH + C_4H_4 \longrightarrow C_4H_3 + H_2O$	1.1×10^{-12}	2	20.7	[26]
56	$OH + C_4H_4O_2 \longrightarrow C_3H_4O + COOH$	5.2×10^{-11}	0	0	[25]
57	$OH + C_4H_4O_2 \longrightarrow C_2H_2O + C_2H_3O_2$	5.2×10^{-11}	0	0	[25]
58	$OH + COOH \longrightarrow CO_2 + H_2O$	1.0×10^{-11}	0	0	[22]
59	$OH + C_2H_2O_2 \longrightarrow CO + HCO + H_2O$	7.0×10^{-12}	0	0	[25]
60	$OH + C_6H_5CHO \longrightarrow$ products	1.4×10^{-11}	0	0	[22]
61	$OH + CH_3 \longrightarrow CH_2O + H_2$	1.7×10^{-12}	0	0	[22]
62	$OH + C_2H_4 \longrightarrow CH_3 + CH_2O$	1.66×10^{-12}	0	−3.8	[28]
63	$OH + C_4H_6 \longrightarrow C_3H_5 + CH_2O$	1.7×10^{-12}	0	0	[29]
64	$OH + C_3H_2 \longrightarrow C_2H_2 + HCO$	8.3×10^{-11}	0	0	[26]
65	$OH + C_2H_2 \longrightarrow C_2H + H_2O$	5.0×10^{-12}	2	58.5	[26]
66	$OH + HO_2 \longrightarrow H_2O + O_2$	1.1×10^{-10}	0	0	[22]
67	$H_2O_2 + H \longrightarrow H_2 + O_2$	4.2×10^{-11}	0	2.9	[18]
68	$H_2O_2 + H \longrightarrow OH + H_2O$	1.7×10^{-15}	0	3.58	[22]
69	$H_2O_2 + H \longrightarrow H_2 + HO_2$	2.8×10^{-12}	0	3.76	[23]
70	$H_2O_2 + O_3 \longrightarrow H_2O + O_2 + O_2$	4.0×10^{-20}	0	0	[22]
71	$H_2O_2 + CH_3O \longrightarrow CH_3OH + HO_2$	5.0×10^{-15}	0	2.59	[22]
72	$H_2O_2 + CH_3O_2 \longrightarrow CH_3OOH + HO_2$	4.0×10^{-12}	0	9.94	[23]
73	$HO_2 + CH_3 \longrightarrow OH + CH_3O$	3.0×10^{-11}	0	0	[22]
74	$HO_2 + CH_2O \longrightarrow HOCH_2OO$	9.7×10^{-15}	0	−5.20	[22]
75	$HO_2 + CH_3O_2 \longrightarrow O_2 + CH_3OOH$	3.8×10^{-13}	0	−6.49	[22]
76	$HO_2 + O_3 \longrightarrow OH + O_2 + O_2$	1.0×10^{-13}	0	10.4	[18]
77	$HO_2 + NO \longrightarrow OH + NO_2$	8.7×10^{-12}	0	−2.0	[18]
78	$HO_2 + CH_3CO \longrightarrow$ products	5.0×10^{-11}	0	0	[22]
79	$HO_2 + HO_2 + N_2 \longrightarrow H_2O_2 + O_2 + N_2$	1.9×10^{-33}	0	−8.15	[22]
80	$HO_2 + NO_3 \longrightarrow O_2 + HNO_3$	1.9×10^{-12}	0	0	[22]
81	$HO_2 + HCO \longrightarrow OH + H + CO_2$	5.0×10^{-11}	0	0	[28]
82	$HO_2 + C_2H_2O_2 \longrightarrow HCOCO + H_2O_2$	5.0×10^{-16}	0	0	[25]
83	$HO_2 + C_2H_2O_2 \longrightarrow HCOCO + H_2O_2$	5.0×10^{-16}	0	0	[25]
84	$HO_2 + C_6H_5CH_2 \longrightarrow C_6H_5 + CH_2O + OH$	8.3×10^{-12}	0	0	[22]
85	$HO_2 + HOCH_2OO \longrightarrow O_2 + HCOOH + H_2O$	3.6×10^{-12}	0	0	[22]
86	$HO_2 + C_2H_2O_2 \longrightarrow HCO + CH_2O_3$	5.0×10^{-16}	0	0	[25]
87	$HO_2 + C_2H_2O_2 \longrightarrow HCO + H_2O_2 + CO$	5.0×10^{-16}	0	0	[25]
88	$NO_3 + H_2O \longrightarrow OH + HNO_3$	2.3×10^{-26}	0	0	[22]

Note: The rate constants of processes are presented in Arrhenius form $k = A(T/298)^n \exp(-E_a/RT)$, where $[A] = \mathrm{cm}^3/(\mathrm{mol\ s})$ for the two-particle processes, $[A] = \mathrm{cm}^6/(\mathrm{mol\ s})$ for three-particle processes, $[T] = \mathrm{K}$, $[E_a] = \mathrm{kJ/mol}$, and $R = 8.31 \times 10^{-3}$ kJ/(mol K) is the universal gas constant.

However, the channels of quenching of the metastable level of xenon (Xe) by water molecules were determined in [20]. It was established that the H_2O molecule dissociates into H and OH with a probability close to unity. The energy of the metastable level of Xe is close to the energy of level $N_2(B^3\Pi_g)$. This suggests that quenching of the $N_2(B^3\Pi_g)$ level by a water molecule is also accompanied by formation of H and OH. These considerations were used when choosing the quenching constants and dissociation channels triggered by collisions of water molecules with $N_2(a'^1\Sigma_u^-)$ and $N_2(E_{sum})$ molecules. The cross sections of interaction of electrons with water molecules were taken from [21].

The ion composition of humid-air plasma at atmospheric pressure is not accurately known so far. Hereinafter, we assume that the main cluster positive ions have the form $H^+(H_2O)_n$ and use only the first member of this series ($n = 1$) H_3O^+ in the model. The appearance of $C_6H_5CH_3$ molecules complicates the situation with sorting of the main positive ions. Some data on the ion composition of the beam plasma of humid air with admixture of toluene at low pressure can be found in [23].

Model [1] included charge-exchange reactions of positive ions O^+, O_2^+, O_4^+, N_2^+, and N_4^+ on $C_6H_5CH_3$ molecules. In this work, we added two more charge-exchange reactions (reactions 22 and 23, Table 1) of H_3O^+ ions on toluene molecules [23]. Calculations showed [1] that contribution of ion-molecular reactions to the mechanism of toluene removal in the $N_2 : O_2$ mixture is small and amounts to several percent. However, the ion composition can influence the value of E/N in the discharge and the efficiency of decomposition of toxic substances thereby.

Under the experimental conditions of this work, recombination of ions occurs via two- and three-body ion–ion recombination. For most pairs of recombining ions, we used the typical dependences of the constants of two-body recombination $k_{2ii} = 4 \times 10^{-7} (300/T)^{0.5}$ cm^3/s and three-body recombination $k_{3ii} = 4 \times 10^{-25} (300/T)^{2.5}$ cm^6/s on gas temperature. Following [18], the resulting coefficients of recombination were calculated according to relation $k = k_{2ii} + M \times k_{3ii}$, where M is the concentration of the third component participating in the reaction. The resulting values of the recombination constants for the ion–ion recombination processes are given in Table 1.

In this work, which is based on the model developed in [1], we also included the electron–ion recombination reactions with participation of the main positive ions N_2^+, N_4^+, O_2^+, O_4^+, $C_6H_5CH_3^+$, and $C_6H_5CH_3H^+$. However, under our experimental conditions, its contribution to neutralization of charges and decomposition of toluene is insignificant.

Computer simulation was performed using the Chemical Workbench software package [30] that allows simultaneous solution of equations of chemical and ion-molecular kinetics, the Boltzmann equation for the electron energy distribution function, and the equation for the translational gas temperature.

An advantage of the glow discharge (as compared to the corona and barrier discharges), which substantially simplifies its modeling, is high spatial uniformity and invariance of its parameters in time. This allowed using the experimentally measured value of the average over discharge gap value of the electric field strength E in the calculations. Note that values of the specific energy deposition in the experiments were small and did not exceed 15 J/L, corresponding to additional gas heating of less than 15 K. Taking into account the above mentioned circumstances, we used the approximation of a constant reduced electric field E/N in the simulations. Using the approximation of constant E/N substantially reduces the error related to uncertainty of ion composition.

In the model of constant E/N, the pulse duration of the discharge is determined by the value of energy deposition. To achieve the experimental values of the energy deposition, the discharge pulse duration had to be set to $\tau_p = 1$–20 μs. This value is substantially smaller than the time of passing of a portion of gas being processed through the discharge area. Hence, we used the following technique in the simulation. The dc discharge was replaced with an equidistant succession of k pulses. In so doing, the total determined from the experiment value of energy deposition into the portion of gas was accumulated evenly over succession of these pulses. It was established that the results of the computer simulation with respect to the amount of decomposed toluene were only weakly dependent on the number of pulses k, which was varied between 1 and 50. For the initial concentration of toluene of 15 ppm, the difference in the results of the computer simulation did not exceed 10%, while at initial concentration of 125 ppm, it was less than 1%.

4. CALCULATED AND EXPERIMENTAL RESULTS AND THEIR DISCUSSION

4.1. Regimes of Gas Discharge in Air at Atmospheric Pressure and Their Electric Characteristics

In order to find an average value of the reduced electric field in the discharge, we used experimental current–voltage characteristics (CVCs). The experimentally reduced CVCs of the studied gas discharge for different water vapor content in the gas flow are shown in Fig. 2 (here, I and U are the discharge current and voltage, respectively). There are two intervals with approximately linear dependence of I/U on the voltage: one in the area of small current, which corresponds to the corona discharge, and the second in the area of high currents, which corresponds to the devel-

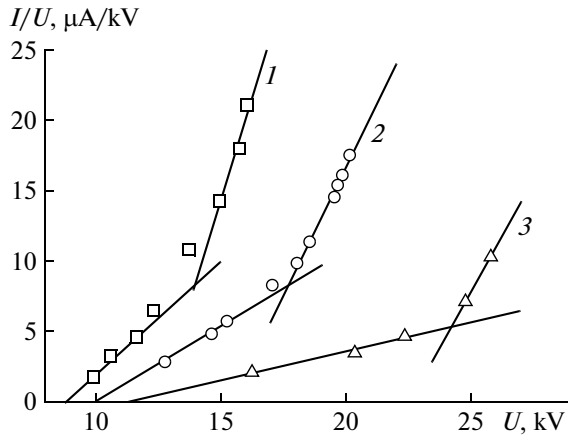

Fig. 2. Experimental reduced current–voltage characteristics of an atmospheric-pressure discharge at an air temperature of $T = 338$ K and different values of humidity ε and flow velocity V: (*1*) ε = 0.7%, V = 15 m/s; (*2*) ε = 10%, V = 15 m/s; (*3*) ε = 18%, V = 20 m/s.

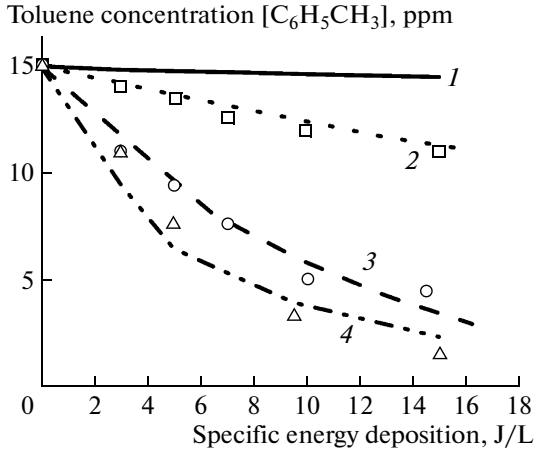

Fig. 3. Calculated (curves) and measured (symbols) concentrations of toluene [$C_6H_5CH_3$] in the plasma chemical reactor as functions of the specific energy deposition for the initial toluene concentration $[C_6H_5CH_3]_0$ = 15 ppm, gas temperature T = 340 K, and different values of humidity ε in the initial gas mixture: ε = (*1*) 0, (*2*) 1.2, (*3*) 10, and (*4*) 18%.

oped glow discharge. The kink area in the reduced CVC (the point where extrapolated straight lines cross each other) can be identified with transition of the negative corona discharge to the glow discharge. The basic physical processes of the gas discharge, evolution electric field, and plasma glow in the gap between the electrodes, which take place under such transition, were studied in detail in [31].

It was found, both experimentally and by computer simulation, that the electric field strength, plasma density, and plasma glow are uniformly distributed in the gap between the electrodes in the developed glow-discharge regime. It can be seen from Fig. 2 that the presence of water vapor in the gas flow substantially increases the voltage of both the corona and glow discharges. This allows us to use the humidity of the working gas as an external controlled parameter for changing the electric field strength in the discharge. Due to the low initial concentration of toluene $[C_6H_5CH_3]_0 \le 125$ ppm, the dependence of E/N on this parameter turned out to be insignificant. Experimental values of E/N used for the calculations are presented in Table 3. At zero humidity, the value of E/N used in the calculations was determined by extrapolation of data of Table 3. When finding the value of the reduced electric field, we assumed that the cathode voltage drop is 300 V.

Table 3. Experimental values of the reduced electric field in a glow discharge used in the simulations

ε, %	1.2	10	18
$(E/N)_{15}$, Td	64	71	71–89
$(E/N)_{125}$, Td	67	74	75–92

$(E/N)_{15}$ and $E/N)_{125}$ stand for the reduced electric fields for initial toluene concentrations of 15 and 125 ppm, respectively.

4.2. Results of Computer Simulations of Toluene Decomposition, Comparison with the Experiment, Analysis of the Main Channels of $C_6H_5CH_3$ Decomposition, and Influence of Humidity

The main characteristic of the efficiency of toluene removal is the quantity of destructed toluene. Figures 3 and 4 illustrate the experimentally determined and calculated concentration of residual toluene in the plasma chemical reactor as a function of specific energy deposition for several values of the initial gas flow humidity and initial toluene content. It can be seen that the results of the calculation describe the experimental data quite well.

The results presented in Figs. 3 and 4 clearly demonstrate the importance of the humidity of the gas flow for increasing the efficiency of its purification from toluene by means of a glow discharge. Water vapor influences the efficiency of toluene decomposition in two ways: by changing the properties and characteristics of the glow discharge and by changing the plasma chemical processes of $C_6H_5CH_3$ decomposition. The availability of electronegative molecules of H_2O leads to the appearance of an additional channel of consumption of electrons via their dissociative attachment to water molecules and, correspondingly, to the increase in the electric field strength in the discharge, as can clearly be seen from the experimental results presented in Figs. 2 and 3. Obviously, the aforementioned factors (a decrease in the electron density and an increase in the electric field strength in the dis-

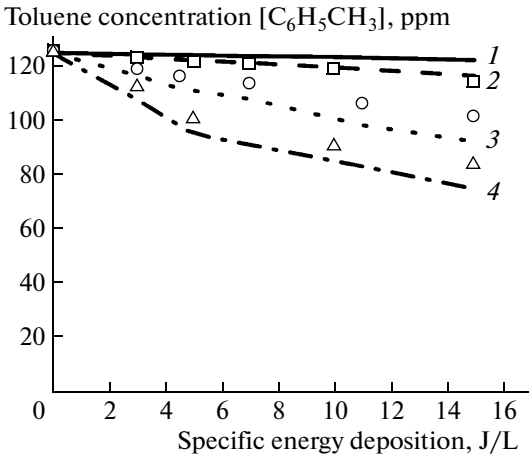

Fig. 4. Calculated (curves) and measured (symbols) toluene concentrations [$C_6H_5CH_3$] in the plasma chemical reactor as functions of the specific energy deposition for the initial toluene concentration $[C_6H_5CH_3]_0 = 125$ ppm, gas temperature $T = 340$ K, and different values of humidityε in the initial gas mixture: ε = (*1*) 0, (*2*) 1.2, (*3*) 10, and (*4*) 18%.

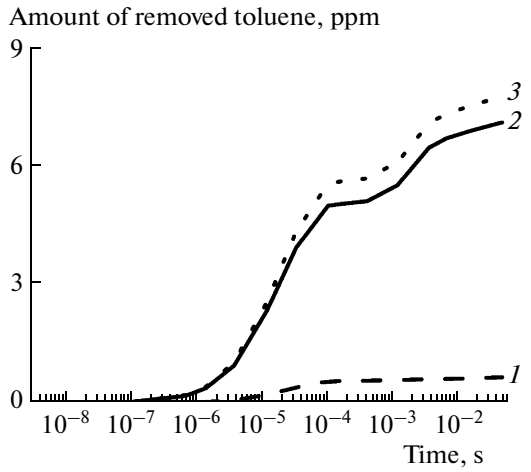

Fig. 5. Contributions of reaction 1 (curve *1*) and reactions 2 and 3 (curve *2*) to toluene decomposition for the initial toluene concentration $[C_6H_5CH_3]_0 = 125$ ppm, gas temperature $T = 340$ K, specific energy deposition is 15 J/L, and flow humidity ε = 1.2%. Curve *3* shows the total removal of $C_6H_5CH_3$.

charge) have opposite influence on the rate of production of chemically active particles and, correspondingly, on the efficiency and degree of toluene removal.

Analysis of the results of computer simulation shows that reactions of toluene with atoms of oxygen O and hydroxyl radical OH were crucially important for decomposition of toluene under our experimental conditions:

$$O + C_6H_5CH_3 \longrightarrow C_6H_5CH_2 + OH, \quad (1)$$

$$OH + C_6H_5CH_3 + N_2 \longrightarrow C_6H_5CH_3OH + N_2, \quad (2)$$

$$OH + C_6H_5CH_3 \longrightarrow C_6H_5CH_2 + H_2O. \quad (3)$$

At gas temperature $T = 340$ K, the total rate constant of interaction of hydroxyl radical OH with a toluene molecule was about two orders of magnitude higher than the rate constant of interaction of $C_6H_5CH_3$ molecules with atoms of oxygen [22]. The calculations show that, in this situation, a substantial fraction of the produced oxygen atoms was used for ozone generation.

Figure 5 illustrates the calculated temporal dynamics of contributions of the main channels of toluene decomposition. As can be seen from Fig. 5, the hydroxyl radical OH whose concentration increases with an increase in humidity is crucial for toluene decomposition in the glow discharge in humid air. Curve *2* in Fig. 5 represents the total contribution of reactions (2) and (3), while, as can be seen from the results of the simulation, the contribution of two-body reaction (3) did not exceed 10%. The calculated ratio of contributions of channels (2) and (3) to the decomposition of toluene is determined by the low gas temperature $T = 340$ K in the glow discharge, for which the rate constant of process (2) is approximately an order of magnitude larger than the rate constant of process (3) [22].

Channel (2), dominant at low temperatures, starts toluene decomposition of toluene. This step consists of the addition of the OH radical to the aromatic ring. Further on, the resulting radical actively interacts with molecular oxygen [1]. Subsequent plasma chemical transformations result in the end products of decomposition (CO_2 and H_2O). The rate constant of reaction (2) decreases, while the rate constant of reaction (3) increases with increasing gas temperature [22]. Hence, in other types of gas discharge at atmospheric pressure, e.g., in the constricted glow, spark, or arc discharge), in which gas temperature T exceeds 1000 K, the ratio of contributions of channels (2) and (3) to decomposition of toluene changes to opposite. Consequently, in the case of high temperatures, the chain of reactions of toluene decomposition can be different.

The contribution of atoms of oxygen to the decomposition of toluene in humid air decreases with an increase in concentration of [H_2O] vapor: it equals 9 and 1.4% for gas humidity levels of 1.2 and 10%, respectively. Metastable molecules of nitrogen $N_2(A^3\Sigma_u^+)$ and $N_2(a'^1\Sigma_u^-)$, which play the key role in decomposition of $C_6H_5CH_3$ in pure nitrogen and make a substantial contribution to the $N_2 : O_2$ mixture with an oxygen content of less than 5%, do not have a noticeable influence on the decomposition of toluene in humid air. Note that the contribution of electronically excited molecules of $N_2(A^3\Sigma_u^+)$, $N_2(a'^1\Sigma_u^-)$, and $N_2(E_{sum})$ (reactions (1)–(3) in Table 2) to the production of hydroxyl radical OH is substantial.

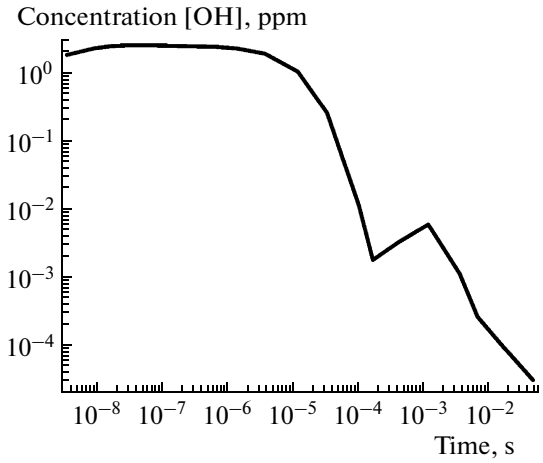

Fig. 6. Calculated temporal dynamics of hydroxyl radical [OH] in the afterglow stage for the initial toluene concentration $[C_6H_5CH_3]_0$ = 125 ppm, gas temperature T = 340 K, specific energy deposition is 15 J/L, and flow humidity ε = 1.2%.

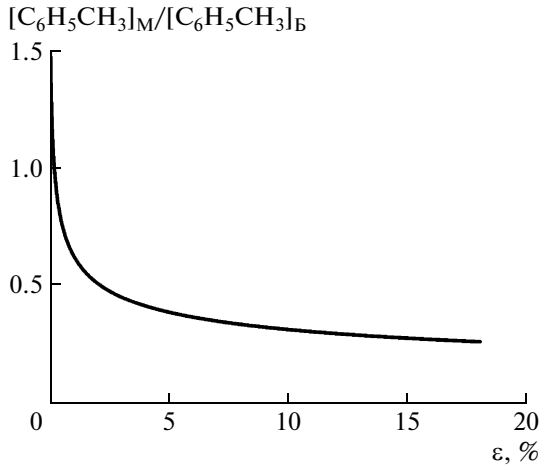

Fig. 7. Calculated ratio $[C_6H_5CH_3]_S/[C_6H_5CH_3]_F$ of the amount of toluene $[C_6H_5CH_3]_S$ removed in the slow (10^{-4}–10^{-2} s) phase to the amount of toluene $[C_6H_5CH_3]_F$ removed in the fast stage (10^{-9}–10^{-4} s) as a function of the flow humidity ε for $[C_6H_5CH_3]_0$ = 125 ppm, T = 340 K, and the specific energy deposition of 15 J/L.

Simultaneous analysis of Figs. 5 and 6, which illustrate temporal dynamics of concentration of the hydroxyl radical [OH] in the afterglow stage, reveals two characteristic stages in the dynamics of toluene decomposition in humid air: a fast one (with a duration of about 100 μs) and a slow one (with a duration of about 100 ms).

In the active discharge stage, the generation of OH radicals is determined by the dissociation of H_2O molecules via direct electronic impact and via collisions with electronically excited nitrogen molecules $N_2(A^3\Sigma_u^+)$, $N_2(a'^1\Sigma_u^-)$, and $N_2(E_{sum})$ or oxygen atoms $O(^1D)$. In the latter case, simultaneously two OH radicals are produced. On the time frame of up to 100 μs in the afterglow stage, OH radicals are produced only in collisions of water molecules with excited particles. At longer times (up to 100 ms), OH is generated in reactions of atomic oxygen with products of decomposition of toluene molecules.

It is seen from Fig. 6 that OH radicals produced in both the active and afterglow stages of the discharge take part in reactions of toluene decomposition. The results of computer simulations reveal a substantial increase in the OH concentration in the early afterglow stage relative to the active discharge stage (up to 50% at moderate levels of flow humidity, ε ~ 1%). When the humidity of the working gas increases, the relative increase in the OH concentration in the afterglow decreases and amounts to about 20% at ε = 10%. This is because reactions of quenching of electronically excited molecules and atoms by H_2O molecules get accelerated at a higher concentration of water vapor, and their contribution is considerable in the active discharge stage.

In the late afterglow stage, the intensity of the reactions of toluene decomposition is two to three orders of magnitude lower than in the fast stage. However, due to the long duration of this stage, its contribution to decomposition of toluene is comparable with that of the fast stage. The curve in Fig. 7 shows the ratio of the contributions of the slow and fast stages as a function of flow humidity. One can see that relative contribution of the slow stage decreases with an increase in water vapor concentration but remains substantial (at a level of 30%) even at ε = 18%.

Analysis of the kinetics of toluene decomposition in the slow stage shows that the main channel of toluene decomposition in this case is also related to reaction $C_6H_5CH_3$ + OH, but the source of the hydroxyl radical in this time interval is different from that in the fast stage. As can clearly be seen from Fig. 6, radical OH produced both in the discharge and the early afterglow stages is practically completely consumed by time t = 100 μs. Further on, at time t > 100 μs, the concentration of OH starts increasing again. The generation of hydroxyl radical OH at this time interval occurs in plasma chemical reactions of conversion of toluene initiated by the glow discharge. The conducted computer simulation showed that, at a fixed value of the flow humidity, the relative contribution of the slow stage increases with an increase in specific energy deposition into the gas and initial content of toluene and amounts to 40–60%.

Figure 8 illustrates the behavior of the energy cost of $C_6H_5CH_3$ molecule decomposition as a function of humidity for different values of the initial toluene concentration. One can see that the energy cost monoton-

ically decreases with an increase in flow humidity. At a high concentration of [H_2O] vapor, the energy cost as a function of concentration of [H_2O] experiences saturation. Comparison of Figs. 3, 4, and 8 shows that the degree of removal of $C_6H_5CH_3$ at a fixed energy deposition decreases with increasing initial toluene content. However, the energy efficiency of the purification process is substantially higher in this case.

The behavior of the energy cost with increasing humidity is directly related to the decomposition mechanism of $C_6H_5CH_3$ caused by its reaction with OH. At a low level of humidity, a higher water vapor concentration leads to a higher reduced electric field and an increase in the concentration of hydroxyl radical [OH], which results in a sharp decrease in the energy cost of $C_6H_5CH_3$ molecule decomposition. The further increase in humidity causes a considerable drop in the electron density in the discharge due to dissociative attachment of electrons to H_2O molecules, the rise in the concentration of hydroxyl radical substantially slows down, and the energy cost decreases more slowly.

The decrease in energy cost upon an increase in the initial concentration of toluene is typical of all electrophysical processes of gas purification. The reason for this behavior lies in the plasma process being nonselective, i.e., there is a large number of channels causing consumption of chemically active particles produced in the discharge. In other words, besides useful channels of consumption of active particles in reactions with toluene molecules, they also vanish in reactions with other molecules and atoms, including reactions of their mutual recombination. Apparently, the relative contribution of such side reactions (undesirable for the purpose of gas purification, because they decrease its energy efficiency) increases upon a decrease in concentration of harmful molecules. The conducted computer simulation showed that reactions of mutual recombination of hydroxyl radicals OH start significantly influencing the balance of the latter when concentration of toluene molecules drops below 5–10 ppm (depending on the flow humidity).

The main channel of the growth of the energy cost of $C_6H_5CH_3$ molecule decomposition under the conditions of glow discharge is related to reaction

$$O + OH \longrightarrow H + O_2, \quad (4)$$

in which two active particles crucial for decomposition of toluene are lost.

4.3. Composition and Concentrations of the Main Products of Toluene Decomposition

Water vapor not only increases the efficiency of toluene removal but also leads to quantitative and qualitative changes in the content of intermediate and final products of $C_6H_5CH_3$ decomposition. For example, the concentration of such a stable intermediate product as acetylene C_2H_2, whose concentration remains sufficiently high and independent of oxygen content in the case of decomposition of $C_6H_5CH_3$ in a dry $N_2 : O_2$ gas mixture [1], substantially drops in a humid flow.

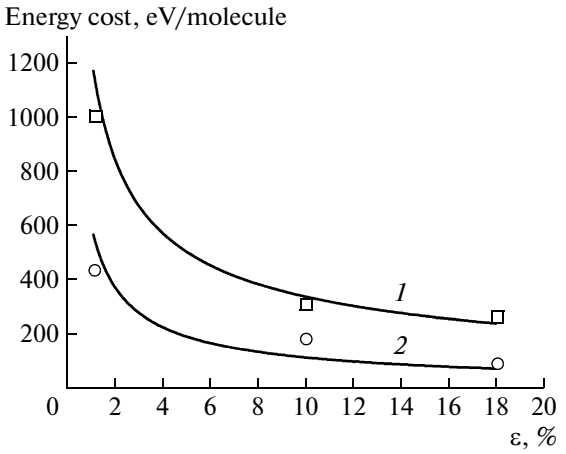

Fig. 8. Calculated (curves) and measured (symbols) energy costs of removal of one $C_6H_5CH_3$ molecule as functions of the humidity ε for the initial toluene concentrations of $[C_6H_5CH_3]_0$ = (*1*) 15 and (*2*) 125 ppm. The specific energy deposition is 10 J/L and the other parameters are the same as in Fig. 2.

Figure 3 illustrates the results of simulation of production of carbon oxides CO and CO_2 for several values of flow humidity. Also shown is the dependence of selectivity S of carbon dioxide yield on humidity [30]:

$$S = [CO_2]/([CO_2] + [CO]). \quad (5)$$

Carbon oxides, along with water, are stable end products of decomposition of volatile organic compounds, and their production is an indication of completeness of toluene oxidation. From the point of view of gas purification, most preferable is obtaining a high yield of carbon dioxide CO_2, which is a less dangerous product than carbon monoxide CO. Selectivity S defined by Eq. (5) is the quantitative indicator of the completeness of oxidation of intermediate products to an ecologically safe stable end product.

As can be seen from Fig. 9, at constant specific energy deposition in the gas, the yield of carbon oxides (CO and CO_2) monotonically increases with an increase in humidity of the gas flow. Analysis of the results of simulation showed that the rate of an increase in the yield of carbon oxides at the output of the plasma chemical reactor substantially exceeds the rate of an increase in decomposition of toluene with increasing water vapor content in the gas. Thus, in dry air (ε = 0%), the ratio of the number of CO and CO_2 molecules at the output of the reactor to the number of destroyed $C_6H_5CH_3$ molecules was 18% (for specific energy deposition of 15 J/L), while at humidity ε = 18%, this ratio was equal to 40%. Hence, an increase in the humidity of the working gas by means of a glow

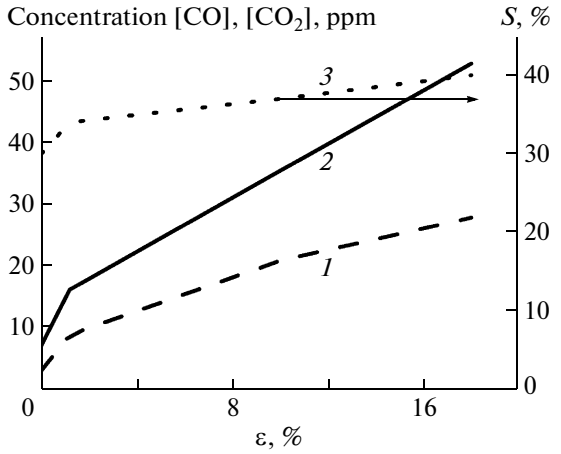

Fig. 9. Calculated dependences of the concentrations $[CO_2]$ (curve *1*) and [CO] (curve *2*) and selectivity *S* of the CO_2 yield (curve *3*) (see formula (5)) at the output of the plasma chemical reactor on the flow humidity ε for the specific energy deposition 100 J/L $[C_6H_5CH_3]_0$ = 125 ppm and $T = 340$ K.

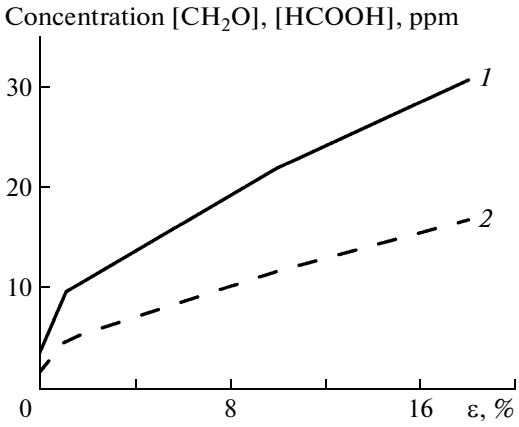

Fig. 10. Concentrations of formaldehyde $[CH_2O]$ (curve *1*) and formic acid [HCOOH] (curve *2*) at the output of the plasma chemical reactor as functions of the flow humidity ε for the specific energy deposition 100 J/L, $[C_6H_5CH_3]_0 = 125$ ppm, and $T = 340$ K.

discharge leads not only to an increase in the amount of decomposed toluene but also to a more complete oxidation of intermediate products to stable CO and CO_2 oxides. Simultaneously, the fraction of CO_2 (selectivity *S*) in total amount of carbon oxides increases. Analysis of mechanisms of formation of carbon oxides within the framework of the kinetic model showed that reaction

$$CO + OH \longrightarrow CO_2 + H. \quad (6)$$

is the major factor causing an increase in CO_2 selectivity.

Alcohols, aldehydes, and carbon acids are typical intermediate products of oxidation of aromatic carbohydrates, including toluene [24]. As an example, Fig. 10 shows the calculated dependences of the concentrations of formaldehyde $[CH_2O]$ and formic acid [HCOOH] on the gas flow humidity at a constant specific energy deposition. The selected products appear closer to the end of the long chain of transformations of $C_6H_5CH_3$ molecule into end products (CO_2 and H_2O), and their efficient production indicates increasing oxidation potential of nonequilibrium low-temperature plasma at higher flow humidity.

Another aldehyde, benzaldehyde C_6H_5CHO, demonstrates a more complex dependence on humidity than CH_2O (Fig. 11). Benzaldehyde is the main aromatic intermediate product of oxidation of toluene, which is detected in all experiments on decomposition of $C_6H_5CH_3$ in oxygen-containing gas mixtures [24]. According to the model developed in [1], benzaldehyde is produced at the beginning of oxidative destruction of the $C_6H_5CH_3$ molecule, which occurs without destruction of the aromatic ring. The first step in production of benzaldehyde includes either reactions (1) and (3), as a result of which there appears benzyl radical $C_6H_5CH_2$ rapidly reacting [24] with either an atom of oxygen O, which results in formation of benzaldehyde:

$$O + C_6H_5CH_2 \longrightarrow C_6H_5CHO + H, \quad (7)$$

or reaction with oxygen molecule O_2 resulting in formation of peroxide radical:

$$C_6H_5CH_2 + O_2 + N_2 \longrightarrow C_6H_5CH_2OO + N_2. \quad (8)$$

Reaction of mutual recombination of peroxide radicals $C_6H_5CH_2OO$ produces benzaldehyde [24].

The experiment [24] showed that the concentration of C_6H_5CHO under decomposition of toluene in a dielectric barrier discharge in dry $N_2 : O_2$ gas mixture changes nonmonotonically with increasing specific energy deposition: initial increase in C_6H_5CHO concentration is followed by its decrease. Model [1] predicts the experimentally established benzaldehyde dynamics [24]. The main channels of decomposition of C_6H_5CHO are related to reactions

$$O + C_6H_5CHO \longrightarrow C_6H_5CO + OH, \quad (9)$$

$$OH + C_6H_5CHO \longrightarrow C_6H_5CO + H_2O. \quad (10)$$

The results of simulation presented in Fig. 11 reflect the complexity of kinetic processes of benzaldehyde dynamics in the presence of water vapor. It can be seen that, at small values of specific energy deposition (15 J/L), an increase in flow humidity leads to growth of $[C_6H_5CHO]$ concentration. The tendency is reversed at large values of the energy deposition (100 J/L).

Figure 12 shows the concentration of benzaldehyde as a function of specific energy deposition at different values of flow humidity. It can be seen that at $\varepsilon = 0\%$ concentration $[C_6H_5CHO]$ monotonically increases with increasing energy deposition. Saturation of the

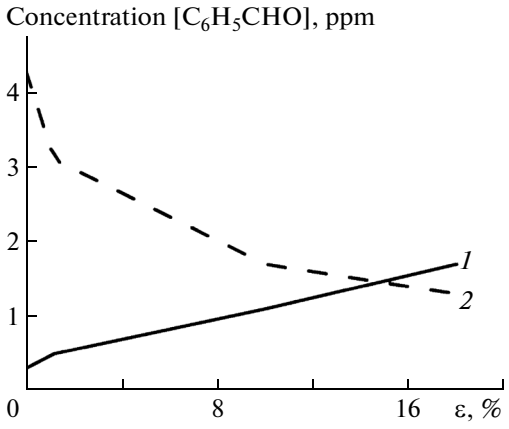

Fig. 11. Calculated concentration of benzaldehyde [C_6H_5CHO] at the output of the plasma chemical reactor as a function of the flow humidity ε for $[C_6H_5CHO]_0$ = 125 ppm, T = 340 K, and specific energy depositions of (*1*) 15 and (*2*) 100 J/L.

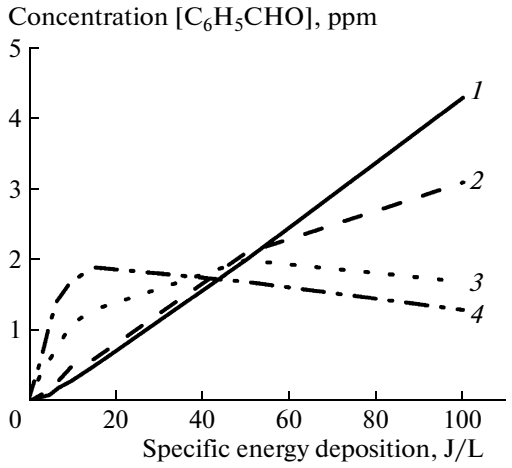

Fig. 12. Calculated benzaldehyde concentration [C_6H_5CHO] at the output of the plasma chemical reactor as a function of specific energy deposition for $[C_6H_5CHO]_0$ = 125 ppm, T = 340 K, and different values of the flow humidity: ε = (*1*) 0, (*2*) 1.2, (*3*) 10, and (*4*) 18%.

growth of [C_6H_5CHO] followed by its subsequent decrease, which was obtained experimentally [24] and predicted by computer simulation [1], occurs at the specific energy deposition of 150–200 J/L. The introduction of water vapor at a low concentration (ε = 1.2%) into plasma forming gas (curve *2*) leads to a noticeable decrease in the growth rate of concentration [C_6H_5CHO] at energy deposition $q > 50$ J/L. Further increase in flow humidity (ε = 10%) causes a decrease in concentration [C_6H_5CHO] at $q > 50$ J/L. A substantial decrease in the growth rate of concentration [C_6H_5CHO] takes place already at $q > 10$ J/L (curve *3*). At a high level of humidity (ε = 18%, curve *4*), instead of growing, the benzaldehyde concentration [C_6H_5CHO] starts to decrease already at q = 15 J/L.

As can be seen from Fig. 12, the specific energy deposition at which [C_6H_5CHO] becomes independent of humidity is $q \sim 45$ J/L (the crossing point of all four curves). Analysis of the kinetic processes within the framework of the developed model sheds light on the mechanism through which humidity influences the benzaldehyde dynamics. An increase in humidity leads to the growth of the number of decomposed toluene molecules and, correspondingly, to an increase in the density of produced radicals [$C_6H_5CH_2$], which, in turn, results in increased concentration [C_6H_5CHO]. Reaction (10) is critical for the decomposition of benzaldehyde molecules C_6H_5CHO under the chosen experimental conditions; the rate of this reaction is about a factor of 25 higher than that of reaction (9).

Interestingly, the rate of interaction of atoms O and radicals OH with the C_6H_5CHO molecule is substantially higher than the analogous rate constants of interaction with the initial $C_6H_5CH_3$ molecule [22]. The equilibrium concentration of benzaldehyde, at which the rate of decomposition of C_6H_5CHO according to reaction (10) becomes equal to the rate of its formation, decreases as the flow humidity becomes higher.

Figure 13 shows the results of computer simulation of production of ozone at the output of the plasma chemical reactor as a function of the humidity of the working gas at different values of the specific energy deposition. Comparison of Fig. 13 and Fig. 11 shows that the dependence of O_3 concentration on humidity is largely similar to the analogous dependence for benzaldehyde. Production of ozone is of special interest in relation to purification of gas flows from toluene. It is known [22] that ozone in the gas phase practically does not interact with $C_6H_5CH_3$: the rate constant of reaction between ozone and toluene is $k = 2 \times 10^{-22}$ cm^3/s. However, as was shown in recent experimental studies [33], the adsorbed toluene is decomposed with high efficiency by ozone in adsorbent pores. Thus, placing an adsorbent at the output of the plasma chemical reactor leads to a substantial increase in the degree of toluene decomposition and energy efficiency of gas purification.

As is well known from practice of ozone generation [34], the presence of water vapor in the gas mixture (oxygen, air) leads to a noticeable decrease in O_3 concentration at the output of the ozone generator. However, currently, complete understanding of the influence of H_2O vapor on ozone formation is lacking. The developed kinetic model allowed establishing the main mechanisms of the influence of water vapor. The increase in [O_3] with an increase in flow humidity at small values of energy deposition is caused by increased reduced electric field E/N in the gas discharge (Fig. 2). Under these conditions, generation of

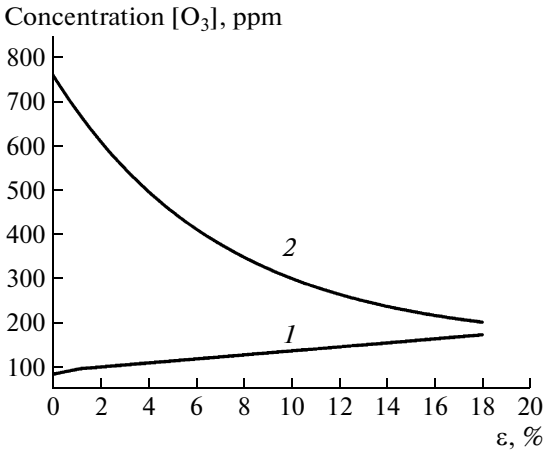

Fig. 13. Calculated ozone concentration $[O_3]$ at the output of the plasma chemical reactor as a function of the flow humidity ε for $[C_6H_5CHO]_0 = 125$ ppm, $T = 340$ K, and specific energy depositions of (*1*) 15 and (*2*) 100 J/L.

atomic oxygen increases, while concentration of products of water dissociation (OH, HO_2, and H_2O_2 radicals) is not high enough to influence the processes of ozone formation.

At a high value of energy deposition, as can be seen from Fig. 13, concentration of O_3 experiences a substantial drop with increasing flow humidity. Calculations showed that, at fixed gas humidity, the degree of reduction of O_3 concentration at the output of the reactor increases with increasing specific energy deposition into the gas. It was established that the main channel of influence of humidity on ozone yield is related to removal of oxygen atoms in a catalytic cycle formed by two fast reactions (4) and (11). An atom of hydrogen H obtained in reaction (4) rapidly enters into reaction

$$O + H + N_2 \longrightarrow OH + N_2. \quad (11)$$

The resulting effect of reactions (4) and (11) can be presented as

$$O + O \longrightarrow O_2. \quad (12)$$

Hydroxyl radical OH plays the role of a catalyst in the reaction of mutual recombination of oxygen atoms substantially accelerating it, while the OH radical itself is not consumed. Note that mutual recombination of oxygen atoms according to channel

$$O + O + M \longrightarrow O_2 + M \quad (13)$$

under experimental conditions occurs much slower (reaction constant $k_{13} \sim (10^{-32}–10^{-34})$ cm^6/s [22]. The existence of the above catalytic cycle was confirmed by the experimental results obtained in [35], where it was shown that the rate of consumption of oxygen atoms significantly increases upon the appearance of H_2O vapor in the air.

Production of nitrogen oxides is a very undesirable process for plasma chemical purification of polluted gas flows, because these oxides are detrimental for human health and the environment. From this point of view, their concentration dynamics upon variation of experimental conditions is of special interest. As was shown in [1], intermediate products of decomposition of toluene actively interact with formed nitrogen oxides. The importance of NO oxide for removal of naphthalene, which is a polycyclic aromatic hydrocarbon, was understood in [36].

Figure 14 shows the calculated dependences of the concentrations of nitrogen oxides N_2O and NO_2, nitrous acid HNO_2, and nitric acid HNO_3 at the output of the plasma chemical reactor on the humidity of the gas flow at a fixed value of energy deposition. It can be seen that the introduction of water vapor does not have any noticeable effect on the yield of nitrous oxide N_2O, while the concentration of nitrogen dioxide NO_2 substantially increases with increasing $[H_2O]$. A rather weak influence of humidity on the resulting concentration of oxide $[N_2O]$ is explained by the slow rate of reaction

$$OH + N_2O \longrightarrow HNO + NO, \quad (14)$$

which is the main channel of N_2O consumption. Under chosen experimental conditions, the rate constant of reaction (14) is 3.8×10^{-17} cm^3/s [18].

Interestingly, the concentration of the third important nitrogen oxide (nitric oxide NO) decreases substantially with increasing flow humidity and appears to be considerably lower (at the level of 0.4 ppm) than $[N_2O]$ and $[NO_2]$. Within the developed kinetic scheme, the decisive influence of water vapor on the dynamics of nitrogen oxides NO and NO_2, along with production of HNO_2 and HNO_3, is determined by reactions

$$OH + NO + M \longrightarrow HNO_2 + M, \quad (15)$$

$$OH + HNO_2 \longrightarrow H_2O + NO_2, \quad (16)$$

$$OH + NO_2 + M \longrightarrow HNO_3 + M, \quad (17)$$

$$OH + HNO_3 \longrightarrow H_2O + NO_3, \quad (18)$$

$$O + NO_3 \longrightarrow O_2 + NO_2. \quad (19)$$

It turned out that the process of quenching of the metastable atom of nitrogen $N(^2D_0)$ by molecule of H_2O according to reaction

$$N(^2D_0) + H_2O \longrightarrow \text{products}, \quad (20)$$

which substantially influenced production of monoxide NO in the pulsed corona discharge [37], does not significantly affect the NO dynamics. This difference is attributed to the value of the reduced electric field, $E/N \le 92$ Td, which is realized in the glow discharge and was used in current calculations. When modeling pulsed corona discharge [37], it was assumed that active particles are mainly produced in the head of the developing streamer, where the value of E/N is much higher than 92 Td. Correspondingly, the concentration of excited nitrogen atom $N(^2D_0)$ is much smaller under

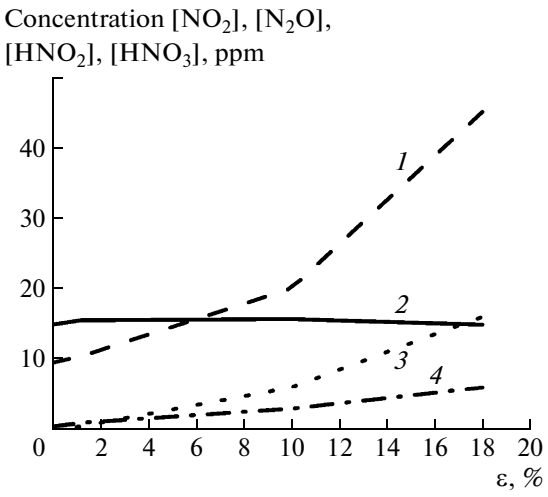

Fig. 14. Concentrations of nitrogen oxides $[NO_2]$ (curve *1*) and $[N_2O]$ (curve *2*), nitrous acid $[HNO_2]$ (curve *3*), and nitric acid $[HNO_3]$ (curve *4*) at the output of the plasma chemical reactor as functions of the flow humidity ε for $[C_6H_5CHO]_0 = 125$ ppm, $T = 340$ K, and specific energy deposition of 100 J/L.

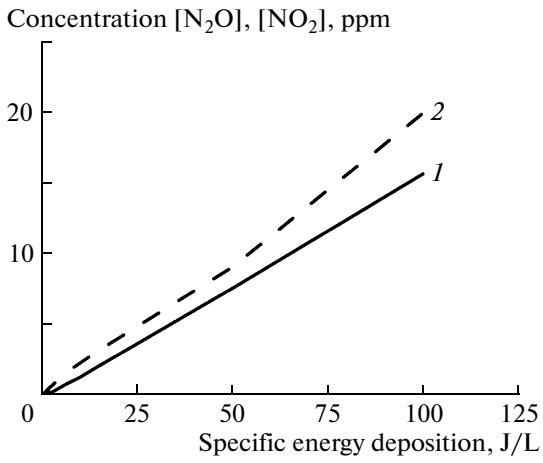

Fig. 15. Concentrations of nitrogen oxides $[N_2O]$ (curve *1*) and $[NO_2]$ (curve *2*) at the output of the plasma chemical reactor as functions of the specific energy deposition for $[C_6H_5CHO]_0 = 125$ ppm, $T = 340$ K, and flow humidity $\varepsilon = 10\%$.

the conditions of glow discharge relative to that in the pulsed corona discharge.

Figure 15 shows the concentration of nitrogen oxides $[N_2O]$ and $[NO_2]$ as a function of specific energy deposition into the gas at fixed humidity. It can be seen that output concentrations of $[N_2O]$ and $[NO_2]$ linearly depend on the deposited energy. While such behavior is expected for N_2O (decomposition of the produced oxide N_2O by the main active particles of O and OH is weak), the linear growth of the concentration of NO_2 is the result of balance between the processes of its formation and decomposition described by Eqs. (16)–(19).

5. CONCLUSIONS

(i) We developed the kinetic model of plasma chemical decomposition of toluene in nonequilibrium low-temperature plasma in the $N_2 : O_2 : H_2O$ mixture. The results of computer simulation are in good agreement with the obtained experimental data on the degree of toluene decomposition in an atmospheric pressure glow discharge.

(ii) The substantial influence of the humidity of the working gas on the efficiency of toluene removal in an atmospheric-pressure glow discharge is demonstrated both experimentally and theoretically. The main mechanisms of the influence of humidity on decomposition of toluene $C_6H_5CH_3$ are determined.

(iii) The major factor in decomposition of $C_6H_5CH_3$ in the glow discharge in the $N_2 : O_2 : H_2O$ mixture is the reaction of the toluene molecule with hydroxyl radical OH. The contribution of oxygen atoms to the removal of $C_6H_5CH_3$ is small and drops with increasing humidity.

(iv) Computer simulations revealed two stages in decomposition of toluene, which differ by duration and intensity of the plasma chemical processes of decomposition of $C_6H_5CH_3$. The first (fast) stage ends in approximately 100 μs after the discharge, while the second (slow) stage continues for several tens of milliseconds.

The main mechanism of decomposition of toluene is the same in both stages. It is related to interaction between $C_6H_5CH_3$ molecules and hydroxyl radical OH, but the sources of OH radicals in these two stages are different. In the fast stage, the hydroxyl radical produced in the glow discharge is consumed in processes of direct electron impact dissociation of water molecules along with interaction of H_2O molecules with electronically excited molecules and atoms of nitrogen and oxygen in the active and afterglow stages of the discharge. The second stage is characterized by a substantially slower relative to the first stage decomposition rate of toluene, which is determined by the intensity of production of the hydroxyl radical in plasma chemical reactions between products of decomposition of $C_6H_5CH_3$ and oxygen atoms.

(v) The relation between the contributions of the fast and slow stages to the total decomposition of toluene depends on the flow humidity, the specific energy deposition into working gas, and the initial toluene content. At a fixed value of energy deposition in the gas, the contribution of the slow stage to toluene decomposition decreases with increasing flow humidity. In so doing, even at the highest humidity ($\varepsilon = 18\%$), this contribution (~30%) is comparable with

the contribution of the fast stage. An increase in the energy deposition and initial toluene content in the gas lead to an increase in the slow-phase contribution to decomposition of $C_6H_5CH_3$.

(vi) The presence of water vapor in the working gas has a significant impact on the composition and dynamics of the intermediate and final products of plasma chemical decomposition of toluene. An increase in flow humidity leads to a noticeable increase in the yield of carbon dioxide CO_2 relative to CO, suppression of yield of acetylene C_2H_2, and a substantial decrease in the yield of ozone. The catalytic cycle, in which hydroxyl radical OH acts as a catalyst, is established. This cycle leads to substantial acceleration of recombination of oxygen atoms and suppression of ozone formation in the presence of water vapor in the plasma-forming gas.

ACKNOWLEDGMENTS

The authors are grateful to N.A. Dyatko, A.P. Napartovich, B.V. Potapkin, S.Ya. Umanskii, and M.A. Deminskii for a fruitful discussion of the results presented in this work. This work was supported by the Russian Foundation for Basic Research (project no. 10-02-01289a).

REFERENCES

1. A. N. Trushkin and I. V. Kochetov, Plasma Phys. Rep. **38**, 407 (2012).
2. A. M. Vandenbroucke, R. Morrent, N. De Geyter, and C. Leys, J. Hazard. Mater. **195**, 30 (2011).
3. R. Rudolph, K. P. Francke, and H. Miessner, Plasma Chem. Plasma Process. **22**, 401 (2002).
4. Yu. S. Akishev, V. B. Karalnik, I. V. Kochetov, et al., in *Proceedings of the 16th International Symposium on Plasma Chemistry, Taormina, 2003*, p. 226.
5. R. Vertriest, R. Morrent, J. Dewulf, et al., Plasma Sources Sci. Technol. **12**, 4121 (2003).
6. H. M. Lee and M. B. Chang, Plasma Chem. Plasma Process. **23**, 541 (2003).
7. Guo Yu-fang, Ye Dai-qi, Chen Ke-fu, and Tian Ya-feng, Chem. Plasma Proc. **26**, 237 (2006).
8. M. Kogoma, Y. Miki, K. Tanaka, and K. Takahashi, Plasma Process. Polym. **3**, 727 (2006).
9. Chang Ming Du, Jian Hua Yan, and B. Cheron, Plasma Sources Sci. Technol. **16**, 791 (2007).
10. J. Van Durme, J. Dewulf, W. Sysmans, et al., Chemosphere **68**, 1821 (2007).
11. N. Blin-Simiand, F. Jorand, Z. Belhadj-Miled, et al., Int. J. Plasma Environ. Sci. Technol. **1**, 64 (2007).
12. R. A. Korzekwa, M. G. Grothaus, R. K. Hutcherson, et al., Rev. Sci. Instrum. **69**, 1886 (1998).
13. S. Futamura, T. Terasawa, and M. Sugasawa, in *Proceedings of the 18th International Symposium on Plasma Chemistry, Kyoto, 2007.*
14. D. N. Chin, C. W. Park, and C. W. Hahn, Bull. Korean Chem. Soc. **21**, 228 (2000).
15. Z. Falkenstein and J. J. Coogan, J. Phys. D **30**, 817 (1997).
16. Y. Akishev, O. Goossens, T. Callebaut, et al., J. Phys. D **34**, 2875 (2001).
17. Y. Akishev, A. Deryugin, I. Kochetov, et al., J. Phys. D **26**, 1632 (1993).
18. Yu. S. Akishev, A. A. Deryugin, V. B. Karal'nik, et al., Plasma Phys. Rep. **20**, 511 (1994).
19. K. H. Becker, E. H. Fink, W. Groth, et al., Faraday Discuss. Chem. Soc., No. 53, 35 (1972).
20. J. Balamuta and M. F. Golde, J. Chem. Phys. **76**, 2430 (1982).
21. Y. Itikawa and N. Mason, J. Phys. Chem. Ref. Data **34**, 1 (2005).
22. J. A. Manion, R. E. Huie, R. D. Levin, et al., *NIST Chemical Kinetics Database, NIST Standard Reference Database 17, Ver. 7.0, Release 1.6.4, Data version 2008.12* (National Inst. of Standards, Technology, Gaithersburg, MD, 2008), http://kinetics.nist.gov/
23. L. W. Sieck, T. J. Buckley, J. T. Herron, and D. S. Green, Plasma Chem. Plasma Process. **21**, 441 (2001).
24. N. Blin-Simiand, F. Jorand, L. Magne, et al., Plasma Chem. Plasma Process. **28**, 429 (2008).
25. *Master Chemical Mechanism* (University of Leeds, Leeds, UK, 2010), http://mcm.leeds.ac.uk/MCM/
26. J. A. Miller and C. F. Melius, Combust. Flame **91**, 21 (1992).
27. R. Knystautas, J. H. S. Lee, J. E. Shepherd, and A. Teodorczyk, Combust. Flame **115**, 424 (1998).
28. H. -Y. Zhang and J. T. McKinnon, Combust. Sci. Technol. **107** (h. 1995), 261.
29. W. J. Pitz and C. K. Westbrook, Combust. Flame **63**, 113 (1986).
30. M. Deminsky, V. Chorkov, G. Belov, et al., Comput. Mater. Sci. **2**, 169 (2003).
31. Yu. S. Akishev, M. E. Grushin, I. V. Kochetov, et al., Plasma Phys. Rep. **26**, 157 (2000).
32. H. H. Kim, A. Ogata, and S. Futamura, J. Phys. D **38**, 1292 (2005).
33. A. Ogata, H. H. Kim, S. M. Oh, et al., in *Proceedings of the International Conference on Electrostatic Precipitation, Cairns, 2006*, p. 1.
34. V. T. Samoilovich, V. I. Gibalov, and K. V. Kozlov, *Physical Chemistry of Barrier Discharge* (Izd. Mosk. Gos. Univ., Moscow, 1989) [in Russian].
35. R. Ono and R. Oda, Int. J. Plasma Environ. Sci. Technol. **1** (h. 2007), 123.
36. V. A. Bityurin, E. A. Filimonova, and G. V. Naidis, IEEE Trans. Plasma Sci. **37**, 911 (2009).
37. M. B. Zheleznyak and E. A. Filimonova, Teplofiz. Vys. Temp. **36**, 557 (1998).

SPELL: OK